EJSIT
European Journal of Science, Innovation and Technology
ISSN: 2786-4936
www.ejsit-journal.com
Volume 3 | Number 4 | 2023

Ab-initio Study of the Structural, Mechanical and Dynamical Properties of Half-Heusler ZrCoY (Y=Sb, Bi) in GW Approximation

Lynet Allan[1*], Winfred M. Mulwa[2], R.E Mapasha[3], Julius M. Mwabora[1], and Robinson J. Musembi[1]
[1]Department of Physics, Faculty of Science and Technology,
University of Nairobi, P.O. Box 30197-00100 Nairobi, Kenya
[2]Department of Physics, Faculty of Science,
Egerton University, P.O Box 536-20115 Egerton, Kenya
[3]Department of Physics,
University of Pretoria, Private Bag x 20, Hatfield, Republic of South Africa

ABSTRACT

In this article, we present an *ab-initio* study of the structural, mechanical, and dynamical stability of ZrCoY (Y=Sb, Bi) using the pseudopotential method within the GW approximation and generalized gradient approximation (GGA). This study employs Density Functional Theory (DFT) to comprehensively investigate the structural, mechanical, electronic, and lattice dynamical properties of cubic Half-Heusler Alloys ZrCoY (Y = Sb, Bi). The structural parameters, namely the equilibrium lattice constant, elastic constant, and its derivative, are consistent with reported experimental and theoretical studies where available. Mechanical properties such as the anisotropy factor A, shear modulus G, bulk modulus B, Young's modulus E, and Poisson's ratio n are calculated using the Voigt-Reuss-Hill average approach based on elastic constants. The Debye temperature, as well as longitudinal and transversal velocities, are predicted from elastic constants at GGA-PBE and GW levels of theory. The study of elastic constants showed that the compounds are mechanically stable, and the phonon dispersion study showed that the materials are dynamically stable. The ductility and anisotropic nature of the compounds were also confirmed by the elastic constants and mechanical properties. This study contributes valuable insights into the potential applications and performance characteristics of ZrCoY (Y=Sb, Bi) Half-Heusler alloys in the field of materials science.

Keywords: First Principles, GW Approximation, Mechanical, Electronic, and Lattice Dynamical Properties, Half-Heusler Alloys, ZrCoY (Y=Sb, Bi)

1 INTRODUCTION

Due to high energy demand, thermoelectric (TE) materials have recently attracted a lot of attention. TE compounds have been found to have the ability to convert heat to electricity in the first instance and electricity back to heat in the second instance. This concept is considerably adopted in cooling and power generation applications (Schierning et al., 2015; Yu et al., 2012; Zhu et al., 2015). Excellent thermoelectric properties have been exhibited by different classes of compounds (Niu et al., 2011; Yu et al., 2012). Interestingly, semiconductor compounds have been identified as the most promising candidates for thermoelectric applications. Semiconductor elements are mainly found in group 3 to 5 of the periodic table. Binary alloys, for example, GaSb and AlSb, exhibit semiconducting properties at room temperature (Strehlow & Cook, 1973). However, several ternary compounds present desirable semiconducting properties compared to binary and elementary semiconductors. Transition metal alloys are regarded as perfectly ordered as well as stable forms of the main class of ternary materials. These transition metal alloys are also known as Heusler alloys, and they

* Corresponding Author lynetamondi3@gmail.com; lynetallan3@students.uonbi.ac.ke

crystallize in a cubic MgAgAs-type structure with space group number 216 (Evers et al., 1997). Heusler alloys are classified into two, that is, Full and Half-Heusler alloys. Full Heuslers (FH) have the atomic composition X_2YZ, while half-Heuslers (HH) have atomic composition XYZ. In both FH and HH alloys, X and Y atoms represent transition metals, while Z stands for semiconductor atoms. HH alloys have attracted researchers' interest due to their wide practical applications in thermoelectric devices, spintronics, and superconductors (Wei & Wang, 2017, 2018; Zeeshan et al., 2017). As a result, new HH compounds are always under study. Nonetheless, the utility of HH alloys has been limited by mechanical and dynamical instability (Legrain et al., 2018). This work is mainly centered on investigating the structural, electronic, mechanical, and dynamical stability of the HH alloys ZrCoSb/Bi, from first principles. Recently, many researchers have focused on HH compounds comprising eighteen valence electrons, employing both the semi-classical Boltzmann technique and density functional theory (DFT). In particular, ZrCoSb has undergone experimental and computational investigations (Sekimoto et al., 2006; Xiao et al., 2018, 2018). Sekimoto and his team predicted the lattice constant and band gaps of MCoSb (M=Ti, Zr, Hf) using experimental techniques. Their findings demonstrated that MCoSb is a semiconductor material with promising thermoelectric properties, aligning with other experimental and computational data (Chauhan et al., 2019; Uher et al., 1999). The most recent report on HH alloys with MNiSn composition (M=Ti, Zr, Hf) (Aliev, 1991; Sakurada & Shutoh, 2005) has positioned them as potential thermoelectric device candidates. Among the studied compounds, Zr-based HH alloys exhibited higher figures of merit (ZT>1) compared to others. However, the stability of MNiSn and MCoSb HH alloys remains unexplored.

For temperature-sensitive applications such as thermoelectrics, understanding the mechanical and dynamical stability of HH compounds is crucial. The ability of these materials to withstand intense and continuous temperature cycling and resist vibrational cracking is vital for their commercialization. Material toughness and mechanical strength serve as indicators of crack resistance. Theoretical calculations can verify a structure's stability by examining its mechanical stability, which is a fundamental condition for thermodynamic and structural stability (Born, 1939) Elastic constants play a significant role in determining mechanical stability, verifying the stability criterion, and assessing other structural parameters (Wu et al., 2017). The quest for fundamental information on how HH materials behave under strain has motivated us to explore elastic properties such as elastic constants.

In the present article, we have made ab initio study of the structural, mechanical, and dynamical stability of ZrCoY (Y=Sb, Bi) using pseudopotential method in GW approximation within generalized gradient approximation (GGA). These properties provide insights into thermal expansion, atomic bonding, as well as potential thermoelectric materials.

The following is an outline of the paper's structure: In Section 2 , we provide the technical details necessary for reproducibility of our computations. A detailed analysis of results and discussions is presented in Section 3. In Section 3.1, we discuss the structural properties of both ZrCoSb and ZrCoBi. The elastic constants and mechanical properties of the compounds under study are outlined in Section 3.2, while the electronic band structures and partial density of states (PDOS) are discussed in Section 3.3. The lattice dynamical properties, including phonon dispersions, are discussed in Section 3.4. Conclusions are presented in Section 4.

2 COMPUTATIONAL DETAILS

In this study, we performed simulations on the cubic HH compounds ZrCoSb and ZrCoBi, both with a=b=c, $\alpha=\beta=\gamma=90°$, using density functional theory (DFT) (Kohn & Sham, 1965) We employed the open-source Quantum ESPRESSO (QE) code (Giannozzi et al., 2009). The Perdew-Burke-Erzenhoff (PBE) flavor of the generalized gradient approximation (GGA) (Perdew et al., 1996) was utilized to account for the core electrons. The electron-ion

interactions were described by ultra-soft pseudopotentials (Kresse & Joubert, 1999). We relaxed the cell to obtain the atomic positions at minimum energy, and the atomic coordinates were relaxed until the forces were less than 0.01 eV/Å. Subsequently, structural optimization of the lattice constant, cut-off energy, and k-points was performed. Experimental lattice parameters were used as the starting point for the optimization process. The data were fitted to the Birch-Murnaghan equation of state (Murnaghan, 1944) and the optimized lattice constants are listed in Table II. Using the calculated lattice constants, the k-points were optimized by fixing the cutoff energy at 30 Ry, which is a small value to keep the computational cost low during test runs. The k-points were varied from a 2x2x2 grid to a dense mesh of 9x9x9. The converged k-point meshes were determined by considering the points with the lowest energy from the graphs. The optimal k-point grid size was found to be 5x5x5 for each of the two compounds.

To obtain an optimal plane wave cutoff energy value, the lattice constants and k-point meshes were set at their optimized values, and the cutoff energy was varied from 20 Ry to 40 Ry. The optimal value was determined to be 30 Ry. Therefore, the wave functions for valence electrons were expanded using a plane-wave basis set within an energy cutoff of 30 Ry, which limited the number of plane waves used. The Kohn-Sham equations were iteratively solved in a self-consistent cycle.

The crystal structures were visualized using the X-window Crystalline and Molecular Structure Visualization (XCrysDen) program (Kokalj & Causà, 2001), and the bond lengths were studied and recorded in Table 1.

The underestimation of band gaps obtained with local density functional theory (DFT) functionals is a well-known issue. This problem can be resolved by using the GW approximation (Atambo et al., 2019), which involves expanding the self-energy in terms of the single-particle Green's function and the screened Coulomb interaction (Reining, 2018). In this study, GW calculations were performed starting from the DFT (PBE) polarizability to calculate the screened interaction W, which was then used to determine the self-energy with the Green function G from DFT (PBE). Such calculations have been reported to be reliable for semiconductor band gaps, which are often underestimated by Kohn-Sham gaps obtained from local DFT calculations (Aoki et al., 2019).

For lattice dynamics, phonon dispersions were studied using six two-dimensional supercells with a total of 24 atoms. The supercells were created using a 3-atom unit cell, with one atom each of Zr, Co, and Bi/Sb for the two compounds under study. The Phonopy code (Togo, 2014) was used to calculate phonons using finite differences.

The elastic constants were calculated using the Thermo-PW post-processing code (Sekimoto et al., 2005) in Quantum ESPRESSO. Before performing all of the above computations, the materials were subjected to variable cell relaxation to ensure they were stress-free. The Lagrangian theory of elasticity, considering the solid as an anisotropic and homogeneous elastic medium (Voigt, 1910), was used to compute the elastic properties within the DFT framework. Due to the cubic symmetry of the materials, there are three independent elastic constants. The Voigt, Reuss, and Hill averaging approaches (Hill, 1952; Reuß, 1929; Voigt, 1910) were used to compute different elastic characteristics using the elastic constants. In Voigt's approximation, the structure is assumed to have uniform strain, while in Reuss' approximation, uniform stress is assumed. Elastic moduli were described using different averaging schemes. In the calculation of the bulk modulus B, which measures the resistance to compressibility, the following expression (Eq. 1) was used:

$$B=\frac{1}{3}(C_{12}+2C_{12}) \quad (1)$$

For Voigt, Reuss, and Hill averages, the bulk modulus for a cubic structure is the same. The Shear modulus, being the deformation that occurs in a solid when a force is applied to one of parallel faces while the other face opposite the parallel face is held in place by opposing forces, is calculated for the cubical symmetry in Voigt average using Eq. (2).

$$G_V = \frac{C_{11}-C_{12}+3C_{44}}{5} \tag{2}$$

The Reuss average is calculated using the expression presented in Eq. (3).

$$G_R = \frac{5(C_{11}-C_{12})C_{44}}{4C_{44}+3(C_{11}-C_{12})} \tag{3}$$

The arithmetic mean of the Voigt and Reuss average in Eq. (4) gives the Hill shear modulus.

$$G_H = \frac{G_V+G_R}{2} \tag{4}$$

Eq. (5) and Eq. (6) are used to compute the Young's modulus and the Poisson's ratio.

$$\gamma = \frac{9BG}{3B+G} \tag{5}$$

$$\eta = \frac{3B-2G}{2(3B+G)} \tag{6}$$

By substituting GV and GR into Eq. 5 and Eq. 6, the Voigt and Reuss averages of Young's modulus and Poisson's ratio were calculated.

By replacing G with G_v and G_r in Eq. (5) and Eq. (6), the Voigt and Reuss averages of Young's modulus and Poisson's ratio are calculated.

Eq. (7) is based on Debye's assumption that the temperature is the highest normal mode of vibration. Debye's temperature is determined from the average sound velocity, as indicated in Eq. (7).

$$\theta_D = \frac{h}{k}\left[\frac{3n}{4\pi}\left(\frac{pN_A}{M}\right)\right]^{\frac{1}{3}}\mu_m \tag{7}$$

where h is the Planck's constant, k is the Boltzmann's constant, NA is the Avogadro's number, n is the number of atoms per molecule or per formula unit, M is the molar mass, p is the density of the unit cell, and μ^m is the average sound velocity.

Eq. (8) further expresses the average sound velocity in terms of compressional (l) and shear (s) sound velocities (Schierning et al., 2015).

$$\mu_m = \left(\frac{1}{3}\right)\left[\frac{2}{u_s^3}+\frac{1}{u_l^3}\right]^{\frac{-1}{3}} \tag{8}$$

Eq. (9) and Eq. (10) respectively give the expressions for μ_s and μ_l.

$$\mu_s = \sqrt{\frac{G}{P}} \tag{9}$$

$$\mu_l = \sqrt{\frac{3B+4G}{3P}} \tag{10}$$

Finally, Equation (11) is used to determine the shear anisotropy (A), which is a measure of the variation in shear properties along different crystallographic directions. The shear anisotropy helps in understanding the type of bonding present in different crystallographic directions.

$$A=\frac{2C_{44}}{C_{11}-C_{12}} \quad (11)$$

These equations are utilized to analyse the elastic properties and bonding characteristics of the ZrCoSb and ZrCoBi compounds in the study.

3 RESULTS AND DISCUSSION

3.1 Structure of ZrCoSb and ZrCoBi

In the study, a cell relaxation calculation was performed to optimize the structure of ZrCoSb and ZrCoBi compounds, as well as the K-points and cut-off energy used in the calculations. The lattice parameters of the crystal structure were estimated based on previous studies of ZrCoY compounds.

To determine the minimum energy configuration, the energy-volume relationship was fitted to the Murnaghan equation of state. By varying the volume, the optimized lattice parameters were obtained. The crystal structure of the ZrCoY alloy was found to be a face-centered cubic (FCC) structure consisting of four interpenetrating sublattices. In the crystal structure, the Zr and Co atoms occupy specific positions known as Wyckoff positions. The Zr atoms are located at (0, 0, 0), the Co atoms at (1/4, 1/4, 1/4), and the Sb/Bi atoms at (1/2, 1/2, 1/2). The fourth sublattice, represented by the vacant positions, is situated at (3/4, 3/4, 3/4).

The crystal structure of the HH ZrCoY alloy is depicted in Figure 1a and Figure 1b, showing the arrangement of atoms in the FCC lattice.

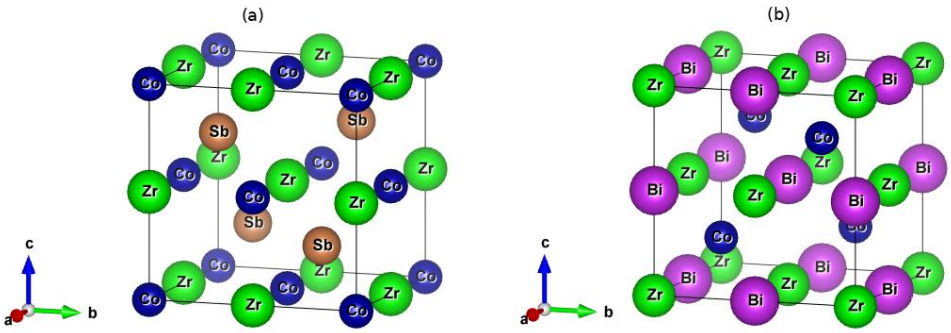

Figure 1: The crystal structures of Half Heusler alloys (a) ZrCoSb and (b) ZrCoBi

After extracting the bond lengths from the optimized crystal structures, they were compared and listed in Table 1. The bond lengths between Co-Sb and Co-Sb/Bi were found to be equivalent and shorter compared to the bond lengths between Zr-Bi/Sb. In general, the bond lengths in the compounds were observed to be shorter, indicating a relatively high bulk modulus. A higher bulk modulus suggests greater resistance to compression, which is indicative of stronger atomic bonding in the material.

Table 1: Calculated bond lengths for ZrCoY (Y=Sb, Bi)

Bonds	Zr-Co	Co-Sb/Bi	Zr-Sb/Bi
Bond Lengths (Å)	2.63	2.64	3.05

Our lattice constants for ZrCoSb agree well with the experimental values of 6.0676 Å obtained by Sekimoto et al. at room temperature (Sekimoto et al., 2005). However, the GW-

calculated lattice parameters provide an improved description of the compounds when compared to the experimental data. The values are listed in Table 3. The optimized and experimental lattice constants show good agreement, as indicated in Table 2. From the table, we observe that the lattice constant of the ZrCoSb compound is approximately 3% smaller than that of ZrCoBi, indicating that the larger mass of Bi causes a slight strain on the Co/Zr atoms. Later, we will discuss how this difference affects the local bonding between the atoms and its influence on the resulting electronic structures. These compounds are narrow-band-gap semiconductors, as predicted by the electronic band structures in Figure 2 and Figure 3.

Table 2: Calculated lattice constants for ZrCoY (Y=Sb,Bi)

Lattice Constant (Å)	**This work**		**GGA**	**Expt**
	GGA	**GWA**		
ZrCoSb	6.01	6.05	6.09 (Joshi *et al.*, 2019)	6.06 (Sekimoto *et al.*, 2005)
ZrCoBi	6.20	6.22	-	-

3.2 Elastic Constants and Mechanical Properties

Table 3 presents the calculated elastic parameters. The estimated values of the elastic constants indicate that both compounds investigated meet the Born-Huang stability criterion (Born, 1939), which states that $C_{11} > 0$, $C_{44} > 0$, $C_{11} - C_{12} > 0$, and $C_{11} + 2C_{12} > 0$. Consequently, the HH compounds ZrCoY (Y=Sb,Bi) are predicted to be mechanically stable.

The C_{11} value for both ZrCoY compounds is higher than C_{12} and C_{44}, suggesting that these compounds are resistant to compression along the X-axes. The computed bulk modulus values for ZrCoSb and ZrCoBi using Eq (1) in the Thermo-PW code are 142.2 GPa and 142.1 GPa, respectively, which are close to the values calculated from Murnaghan's equation of state (136.6 GPa and 136.1 GPa).

The high bulk modulus of 142.2 GPa indicates that ZrCoSb is incompressible, indicating strong bond strength. The calculated shear moduli for ZrCoSb and ZrCoBi are 79.9 GPa and 71.3 GPa, respectively, indicating good hardness. The GW-computed elastic constants are in reasonably good agreement with the GGA-PBE calculations, suggesting that the GW approximation does not significantly affect the bonding of the atoms in the systems.

Unfortunately, there are no elastic constant or elastic modulus results available for ZrCoBi, making a direct comparison challenging. The calculated Young's modulus values are 202.6 GPa for ZrCoSb and 183.4 GPa for ZrCoBi, confirming that ZrCoSb is stiffer than ZrCoBi. The ratio of bulk modulus to shear modulus (B/G), known as Pugh's ratio, is used to assess the ductility of materials. A B/G ratio greater than 1.75 suggests ductility, while a ratio less than 1.75 indicates brittleness. For ZrCoBi and ZrCoSb, the B/G ratios are 1.77 and 1.99, respectively, indicating that the materials are ductile.

Additionally, the Poisson's ratio (ν) is another indicator of ductility. A ν value greater than 0.26 suggests ductility, while a value less than 0.26 indicates brittleness. The calculated values of ν are 0.267 for ZrCoBi and 0.285 for ZrCoSb, confirming the ductility of these materials.

Regarding ZrCoSb, our predicted Young's modulus is approximately 2% higher than the experimental results (Sekimoto et al., 2005). The high value of Young's modulus suggests a dominant covalent bonding component, indicating a strong covalent bond in the material.

The Debye temperature (Θ_D), as well as the compressional and shear wave velocities, were computed and found to be in good agreement with theoretical and experimental data

where available, as outlined in Table 4. The Debye temperature is a fundamental parameter strongly associated with the melting point and specific heats in solids.

From Table 4, the Θ_D (Debye temperature) in ZrCoSb is greater than in ZrCoBi. The Θ_D value for ZrCoSb is in excellent agreement with the experimental values in Table IV, while we report, for the first time, the Θ_D for ZrCoBi. High Debye temperatures indicate a stiffer crystal orientation and are associated with high melting points. In such crystals, a significant amount of energy is required to excite the phonons, making them ideal for thermoelectric power generation.

Moreover, a Debye temperature of 300 K or higher suggests high thermal conductivity in the crystal. Since the studied compounds have Debye temperatures of 392.8 K for ZrCoSb and 323.7 K for ZrCoBi, we can conclude that their thermal conductivity is high.

Additionally, we calculated the shear anisotropy (A) values of 0.72 and 0.63 for ZrCoSb and ZrCoBi, respectively, at the GGA-PBE level, and 0.71 and 0.60 at the GW level of theory. As shown in Table IV, the calculated values of A are either greater than or less than 1, but not equal to 1. In isotropic crystals, the value of A is 1. Therefore, the HH ZrCoY compounds are purely anisotropic, and their shear anisotropy is measured by values different from 1.

Table 3: Calculated elastic constants, Bulk modulus (B), Shear modulus (G), Young's modulus (E), Pugh's ratio (B/G), and Poisson's ratio (n)

Ref	***n***	***E_H (GPa)***	***B/G***	**G_H (GPa)**	***B_H (GPa)***	***C_{44} (GPa)***	***C_{12} (GPa)***	***C_{11} (GPa)***	***Comp***
This work, GGA-PBE	0.262	202.0	1.77	79.9	142.2	69.7	76.9	272.8	ZrCoSb
GGA-PBE (Joshi *et al.,* 2019)	0.25	202.3	1.77	79.3	140.8	70.7	78.1	273.0	
Expt (Sekimoto *et al.,* 2005)	-	201		-	-	-	-	-	
This work, GGA-PBE	0.285	183.1	1.99	71.2	142.1	58.1	77.9	270.6	ZrCoBi

Table 4: The compressional (V_l) and shear wave (V_s) velocity in m/s, Debye's temperature Θ_D in K and the shear anisotropy (A) for ZrCoY

Ref	**A**	***Θ_D***	***v_s***	***v_l***	**Comp**
This work, GGA-PBE	0.72	392.8	3168.6	5589.9	ZrCoSb
GGA-PBE (Joshi *et al.,* 2019)	0.88	392.1	3379.2	5544.1	
Expt (Sekimoto *et al.,* 2005)	-	392.0	3132 .0	5488.0	
This work, GGA-PBE	0.63	323.7	2631.2	4801.0	ZrCoBi

The ZrCoBi compounds exhibit lower sound velocities and Young's modulus compared to ZrCoSb. This difference arises from the weaker chemical bonding and the heavier atomic mass of Bi. The strong relativistic effect of Bi causes contraction of its outer shell and increases its inertness for bonding. As a result, the lower sound velocities and Young's modulus in ZrCoBi contribute to an inherently low lattice thermal conductivity. The weaker bonding and heavier atom in ZrCoBi lead to reduced vibrational energy transfer and thus lower thermal

conductivity in comparison to ZrCoSb. The electronic properties of ZrCoSb and ZrCoBi were analyzed through first-principles calculations, focusing on their band structures and projected density of states.

3.3 Band Structure and Projected Density of States

Figure 2a and Figure 3a present the electronic band structures of ZrCoSb and ZrCoBi, respectively. In both compounds, the valence band maxima (VBM) are located at the Γ point, while the conduction band minima (CBm) are found at the X point. This indicates that the compounds are indirect Γ-X bandgap semiconductors. The bandgaps in these compounds are slightly above 1 eV, making them electronically non-metallic. Additionally, the bandgaps suggest a high reflectivity in the infrared portion of the photon energy spectrum.

The projected density of states, shown in Figure 2b and Figure 3b, provides insights into the distribution of electronic states in the compounds. This analysis helps understand the contributions of different elements to the electronic structure and provides information about bonding and electronic behavior.

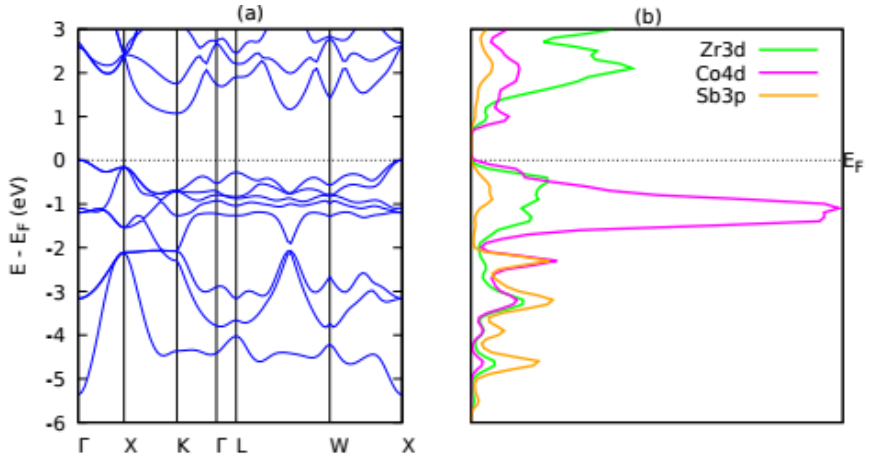

Figure 2: (a) GGA-PBE Calculated Band structures and (b) Projected Density of States (PDOS) for ZrCoSb

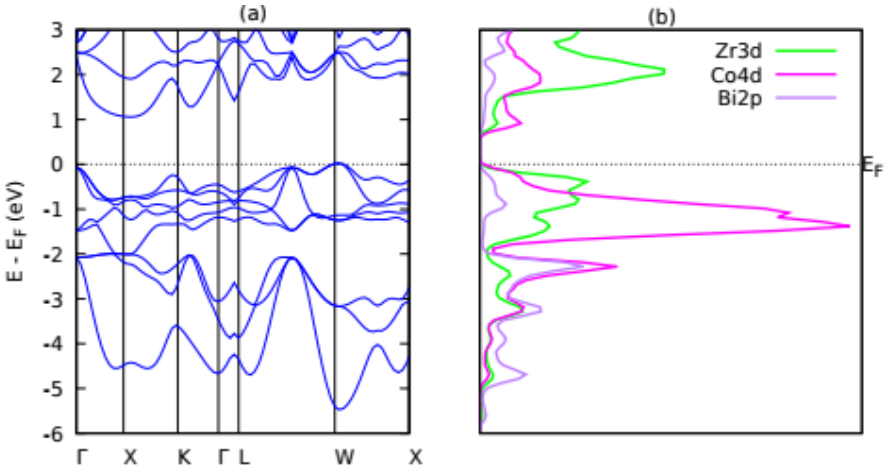

Figure 3: (a) GGA-PBE Calculated Band structures and (b) Projected Density of States (PDOS) for ZrCoBi

Overall, the electronic properties of ZrCoSb and ZrCoBi reveal their semiconductor nature with indirect bandgaps, and the GW approximation yields more accurate bandgap values.

The projected density of states analysis further enhances our understanding of the electronic structure and bonding in these compounds.

The projected densities of states in Figure 2b and Figure 3b. The analysis of the projected density of states reveals the dominance of Zr in both the valence and conduction bands of the alloys. However, in the case of ZrCoBi, the valence state is primarily dominated by Bi in the energy range of -6 to -2 eV. This indicates that Bi plays a significant role in the electronic structure of ZrCoBi. Furthermore, the projected density of states shows a sharp increase in the density of states near the valence band maximum for ZrCoBi. This high density of states suggests a high thermal power in the material. The increased density of states indicates a larger number of available electronic states, which can contribute to enhanced thermoelectric properties such as high thermal conductivity or improved electrical conductivity. Therefore, the dominance of Zr in the valence and conduction bands of the alloys and sharp increase in density of states near the valence band maximum in ZrCoBi point towards its potential for high thermal power and favorable thermoelectric properties.

Table 5: Calculated bandgaps using GGA-PBE in comparison to GW Approximation gaps

Band gap (eV)			**Compounds**
Expt	**This work**		
	GWA	**GGA**	
1.45 (Sekimoto *et al.,* 2005)	1.44	1.05	ZrCoSb
-	1.35	1.03	ZrCoBi

Table 5 summarizes the calculated bandgaps using the GGA-PBE and GW approximations. It is observed that the GW approximation provides a better prediction of the bandgaps compared to the GGA-PBE approximation.

3.4 Lattice Dynamics: Phonon Dispersion

Phonon frequencies are created when atoms in a crystal are displaced from their rest positions, causing pressures to increase (Togo & Tanaka, 2015). Though crystals are expected to be fixed, temperature increase can cause the atoms to vibrate about their mean position. It is important to study how atoms in a crystal vibrate when displaced from their equilibrium positions. This phenomenon affects the stability of alloys, especially at high temperatures, as the fixed lattice structure can experience vibrations due to thermal energy. The analysis of lattice vibrations also provides insights into the energy absorption behavior of solids. In Figure 4(a)-(d), we present the calculated phonon dispersion curves and density of states for ZrCoSb and ZrCoBi.

In our investigation, we considered the unit cell of the alloys, which contains three atoms. To ensure convergence, we constructed a 2 × 2 × 2 supercell for each compound. The computations were carried out in the first Brillouin zone, which represents the primitive cell in the reciprocal lattice. The zones sampled in this study covered Γ - X - U - K - Γ- L - W – X. To determine the dynamical stability of the alloys, we examined the potential energy of the system as a function of atom displacements. If the potential energy continuously increases for all possible combinations of displacements, the system is considered dynamically stable at equilibrium. Thus, phonons should exhibit non-negative and real frequencies to indicate stability. Negative frequencies indicate a decrease in potential energy and therefore signify

instability. Both alloys, ZrCoSb and ZrCoBi, were found to be dynamically stable. This is evident from Figures 4(a-d), where no negative frequencies or dispersions are observed. Considering the presence of three atoms, we expect nine modes in the phonon dispersion spectra (Figures 4(a-b)): three acoustic modes (3) and six optical modes (3n-3). The optical modes are capable of interacting with light. For ZrCoBi, the optical mode occurs between 250-330 cm^{-1}, corresponding to a wavelength range of 30303 nm to 40000 nm. In the case of ZrCoSb, the optical mode frequency range is between 230-300 cm^{-1}. Both alloys exhibit far-infrared frequencies, requiring higher frequencies to bring them into the visible region, which is desirable for solar systems. The maximum frequency for ZrCoBi slightly exceeds 300 cm^{-1}, while for ZrCoSb, it is slightly below 300 cm^{-1}. This difference can be attributed to the heavier mass of Bi compared to Sb. A distinct gap can be observed between the acoustic and optical modes in both alloys, as well as an additional gap between the two optical modes in ZrCoSb. These data are crucial for studying thermal and electrical conductivity and determining the thermoelectric properties of materials.

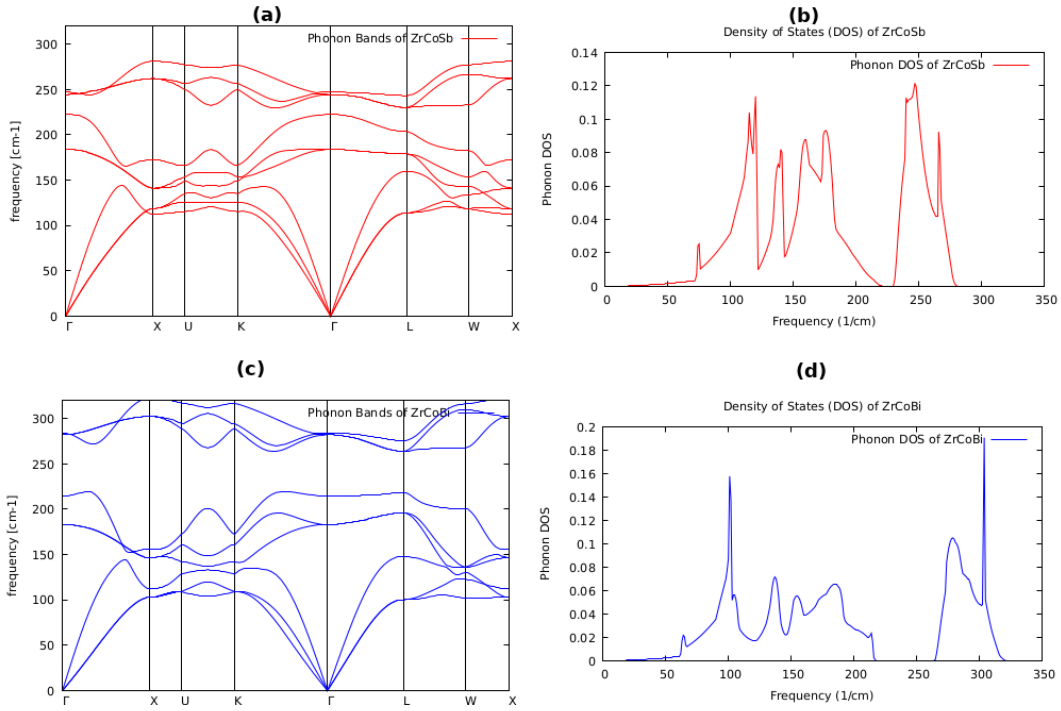

Figure 4: Phonon dispersion Curves for (a) ZrCoSb, (b) ZrCoBi and Density of states for (c) ZrCoSb, and (d) ZrCoB

4 CONCLUSION

In conclusion, we have presented first-principles results on the structural, electronic, mechanical, and lattice dynamical properties of the half-Heusler alloys, ZrCoSb and ZrCoBi. These properties were calculated using the density functional theory (DFT) framework with the GGA-PBE approximation as well as the more advanced GW approximation. Our calculations of elastic constants and mechanical properties using both approaches yielded similar results, which were also in good agreement with available experimental data. However, when it comes to band gaps, the GW approximation provided values that were closer to the experimental data compared to the GGA-PBE calculations. This highlights the importance of employing the GW approach for assessing not only the electronic properties but also the mechanical properties of the half-Heusler family. The computed values of bulk modulus, shear modulus, and Young's modulus confirmed the bond strength, hardness, and stiffness of ZrCoY

alloys, respectively. The bulk modulus values obtained from the Thermo-PW code closely matched those calculated from Murnaghan's equation of state. Additionally, we have presented the elastic constants and Debye's temperature for ZrCoBi for the first time, indicating its mechanical and thermal properties.

Both ZrCoSb and ZrCoBi alloys exhibited relatively high Debye's temperatures, suggesting high thermal conductivity. Furthermore, our analysis indicated that the compounds are mechanically and dynamically stable. The ZrCoY alloys (Y=Bi, Sb) were found to be anisotropic and ductile. The properties of these compounds suggest that further investigation of their transport properties, particularly using the GW approximation, is necessary.

In summary, our study provides valuable insights into the structural, electronic, mechanical, and lattice dynamical properties of ZrCoSb and ZrCoBi half-Heusler alloys, emphasizing the importance of employing advanced computational methods for a comprehensive understanding of these materials.

ACKNOWLEDGEMENT

The authors would like to acknowledge the support received from the Partnership for Skills in Applied Sciences, Engineering and Technology (PASET) through the Regional Scholarship and Innovation Fund (RSIF). The authors would also like to express their gratitude to the Centre of High-Performance Computing (CHPC) in Rosebank, Cape Town, Republic of South Africa, for providing access to the HPC cluster facility used in this research.

DATA AVAILABILITY

The data obtained in this study are available and can be provided upon request to the corresponding author.

REFERENCES

Aliev, F. (1991). Gap at Fermi level in some new d-and f-electron intermetallic compounds. *Physica B: Condensed Matter*, *171*(1–4), 199–205. https://www.sciencedirect.com/science/article/pii/092145269190516H

Born, M. (1939). Thermodynamics of crystals and melting. *The Journal of Chemical Physics*, *7*(8), 591–603. https://aip.scitation.org/doi/abs/10.1063/1.1750497

Chauhan, N. S., Bathula, S., Vishwakarma, A., Bhardwaj, R., Johari, K. K., Gahtori, B., & Dhar, A. (2019). Enhanced thermoelectric performance in p-type ZrCoSb based half-Heusler alloys employing nanostructuring and compositional modulation. *Journal of Materiomics*, *5*(1), 94–102. https://www.sciencedirect.com/science/article/pii/S2352847818300972

Evers, C. B., Richter, C. G., Hartjes, K., & Jeitschko, W. (1997). Ternary transition metal antimonides and bismuthides with MgAgAs-type and filled NiAs-type structure. *Journal of Alloys and Compounds*, *252*(1–2), 93–97. https://www.sciencedirect.com/science/article/pii/S0925838896026163

Joshi, H., Rai, D. P., Hnamte, L., Laref, A., & Thapa, R. K. (2019). A theoretical analysis of elastic and optical properties of half Heusler MCoSb (M= Ti, Zr and Hf). *Heliyon*, *5*(3).

Legrain, F., Carrete, J., van Roekeghem, A., Madsen, G. K., & Mingo, N. (2018). Materials screening for the discovery of new half-Heuslers: Machine learning versus ab initio methods. *The Journal of Physical Chemistry B*, *122*(2), 625–632. https://pubs.acs.org/doi/abs/10.1021/acs.jpcb.7b05296

Niu, M., Xu, W., Shao, X., & Cheng, D. (2011). Enhanced photoelectrochemical performance of rutile TiO2 by Sb-N donor-acceptor coincorporation from first principles calculations. *Applied Physics Letters*, *99*(20), 203111. https://doi.org/10.1088

Sakurada, S., & Shutoh, N. (2005). Effect of Ti substitution on the thermoelectric properties of (Zr, Hf) NiSn half-Heusler compounds. *Applied Physics Letters*, *86*(8), 082105. https://aip.scitation.org/doi/abs/10.1063/1.1868063

Schierning, G., Chavez, R., Schmechel, R., Balke, B., Rogl, G., & Rogl, P. (2015). Concepts for medium-high to high temperature thermoelectric heat-to-electricity conversion: A review of selected materials and basic considerations of module design. *Translational Materials Research*, *2*(2), 025001. https://iopscience.iop.org/article/10.1088/2053-1613/2/2/025001/meta

Sekimoto, T., Kurosaki, K., Muta, H., & Yamanaka, S. (2006). Thermoelectric and thermophysical properties of TiCoSb-ZrCoSb-HfCoSb pseudo ternary system prepared by spark plasma sintering. *Materials Transactions*, *47*(6), 1445–1448. https://www.jstage.jst.go.jp/article/matertrans/47/6/47_6_1445/_article/-char/ja/

Strehlow, W., & Cook, E. L. (1973). Compilation of energy band gaps in elemental and binary compound semiconductors and insulators. *Journal of Physical and Chemical Reference Data*, *2*(1), 163–200. https://aip.scitation.org/doi/abs/10.1063/1.3253115

Uher, C., Yang, J., Hu, S., Morelli, D. T., & Meisner, G. P. (1999). Transport properties of pure and doped MNiSn (M=Zr, Hf). *Phys. Rev. B*, *59*(13), 8615–8621. https://doi.org/10.1103/PhysRevB.59.8615

Wei, J., & Wang, G. (2017). Properties of half-Heusler compounds TaIrGe by using first-principles calculations. *Applied Physics A*, *123*(5), 1–6. https://link.springer.com/article/10.1007/s00339-017-0990-6

Wei, J., & Wang, G. (2018). Thermoelectric and optical properties of half-Heusler compound TaCoSn: A first-principle study. *Journal of Alloys and Compounds*, *757*, 118–123. https://www.sciencedirect.com/science/article/pii/S0925838818317158

Xiao, H., Hu, T., Liu, W., Zhu, Y., Li, P., Mu, G., Su, J., Li, K., & Mao, Z. (2018). Superconductivity in the half-Heusler compound TbPdBi. *Physical Review B*, *97*(22), 224511. https://journals.aps.org/prb/abstract/10.1103/PhysRevB.97.224511

Yu, B., Zebarjadi, M., Wang, H., Lukas, K., Wang, H., Wang, D., Opeil, C., Dresselhaus, M., Chen, G., & Ren, Z. (2012). Enhancement of thermoelectric properties by modulation-doping in silicon germanium alloy nanocomposites. *Nano Letters*, *12*(4), 2077–2082. https://pubs.acs.org/doi/abs/10.1021/nl3003045

Zeeshan, M., Singh, H. K., van den Brink, J., & Kandpal, H. C. (2017). Ab initio design of new cobalt-based half-Heusler materials for thermoelectric applications. *Physical Review Materials*, *1*(7), 075407. https://journals.aps.org/prmaterials/abstract/10.1103/PhysRevMaterials.1.075407

Zhu, T., Fu, C., Xie, H., Liu, Y., & Zhao, X. (2015). High efficiency half-Heusler thermoelectric materials for energy harvesting. *Advanced Energy Materials*, *5*(19), 1500588. https://onlinelibrary.wiley.com/doi/abs/10.1002/aenm.201500588